

Highlights

Process-Informed Forecasting of Complex Thermal Dynamics in Pharmaceutical Manufacturing

Ramona Rubini, Siavash Khodakarami, Aniruddha Bora, George Em Karniadakis, Michele Dassisti

- We formulate an idealized, process-informed trajectory prior and compare three different loss function formulations for deep learning models: a fixed-weight loss, a dynamic uncertainty-based loss and a Residual-Based Attention (RBA) mechanism.
- We compare process-informed forecasting models with a wide range of traditional and state-of-the-art data-driven counterparts. To ensure fairness and clarity, all deep learning architectures are calibrated to the same parameter count. Our evaluation assesses not only predictive accuracy but also physical plausibility and robustness to sensor noise.
- Moreover, we validate the practical utility of our methodology through a transfer learning study, assessing the generalizability of the best-performing model on a new, unseen temperature dynamics.

Process-Informed Forecasting of Complex Thermal Dynamics in Pharmaceutical Manufacturing

Ramona Rubini^{a,b,c,*}, Siavash Khodakarami^c, Aniruddha Bora^c, George Em Karniadakis^c, Michele Dassisti^b

^a*Department of Agricultural and Environmental Sciences, University of Bari, Bari, 70121, Italy*

^b*Department of Mechanical, Mathematics, and Management (DMMM), Polytechnic University of Bari, Bari, 70126, Italy*

^c*Division of Applied Mathematics, Brown University, Providence, 02912, RI, USA*

Abstract

Accurate time-series forecasting for complex physical systems is the backbone of modern industrial monitoring and control. While deep learning models excel at capturing complex dynamics, currently, their deployment is limited due to physical inconsistency and robustness, hence constraining their reliability in regulated environments. We introduce process-informed forecasting (PIF) models for temperature in pharmaceutical lyophilization. We investigate a wide range of models, from classical ones such as Autoregressive Integrated Moving Average Model (ARIMA) and Exponential Smoothing Model (ETS), to modern deep learning architectures, including Kolmogorov-Arnold Networks (KANs). We compare three different loss function formulations that integrate a process-informed trajectory prior: a fixed-weight loss, a dynamic uncertainty-based loss, and a Residual-Based Attention (RBA) mechanism. We evaluate all models not only for accuracy and physical consistency but also for robustness to sensor noise. Furthermore, we test the practical generalizability of the best model in a transfer learning scenario on a new process. Our results show that PIF models outperform their data-driven counterparts in terms of accuracy, physical plausibility and noise resilience. This work provides a roadmap for developing reliable and generalizable forecast-

*ramona.rubini@uniba.it, ramona_rubini@brown.edu

Email addresses: siavash_khodakarami@brown.edu (Siavash Khodakarami), aniruddha_bora@brown.edu (Aniruddha Bora), george_karniadakis@brown.edu (George Em Karniadakis), michele.dassisti@poliba.it (Michele Dassisti)

ing solutions for critical applications in the pharmaceutical manufacturing landscape.

Keywords:

Time-series forecasting, Lyophilization, Kolmogorov-Arnold Networks, Thermal Dynamics, Deep Learning

1. Introduction

In pharmaceutical manufacturing, robust time series forecasting is key to ensuring product quality, process optimization, and predictive maintenance to prevent costly production disruptions. A particularly critical process in this industry is lyophilization, or freeze-drying, used to preserve and stabilize sensitive pharmaceutical products such as vaccines, antibiotics, and biologics. In this process, the moisture of the product is removed at low temperature through sublimation [1]. Given the thermal sensitivity of pharmaceutical products, accurate prediction and control of product temperature during lyophilization are critical [2, 3]. Classical statistical methods like Autoregressive Integrated Moving Average (ARIMA) and Exponential Smoothing (ETS) have been the benchmark for forecasting applications, valued for their simplicity, interpretability, and effectiveness in linear or trend-based data [4, 5, 6, 7, 8, 9, 10, 11, 12].

However, classical approaches are no longer sufficient to capture the complex nonlinear thermal dynamics of physical systems in real-world contexts [13, 14, 15]. This data-rich environment has triggered a paradigm shift to deep learning. In particular, Long Short-Term Memory (LSTM) and the more recent attention-based Transformers have emerged as powerful alternatives to model temporal dependencies and often outperform classical methods [16, 17, 18, 19, 20, 21, 22]. Up to now, these data-driven models ignore the underlying physics of processes. Moreover, their core self-attention mechanism is fundamentally misaligned with the ordered nature of time series [23]. This lack of interpretability can compromise their generalizability, data efficiency and reliability, especially in the pharmaceutical industry, which is subject to strict Good x Practice (GxP) regulations. To bridge the gap between data-driven power and scientific rigor, recent advances have introduced Physics-Informed Neural Networks (PINNs), which incorporate physical knowledge directly into the learning process [24]. This integration guides the model towards physically consistent solutions, even in the presence of sparse or

noisy input, therefore improving its understanding and robustness. A further innovation has come through the development of Kolmogorov-Arnold Networks (KANs) [25]. Inspired by the Kolmogorov-Arnold representation theorem, KANs have learnable univariate activation functions on the edges of the network that improve interpretability and parameter efficiency compared to traditional Multi-Layer Perceptrons (MLPs) [26, 27]. Extensions such as the Chebyshev polynomial-based (cKAN) and models like Long Expressive Memory (LEM) address additional limitations, such as spectral bias leading to accurate modeling of high-frequency dynamics [28, 29, 30].

Building upon these advancements, this paper introduces Process-Informed Forecasting (PIF) models for pharmaceutical freeze-drying. Our main contributions can be summarized as follows:

- We formulate an idealized, process-informed trajectory prior and compare three different loss function formulations for deep learning models: a fixed-weight loss, a dynamic uncertainty-based loss [31] and a Residual-Based Attention (RBA) mechanism [32].
- We compare PIF models with a wide range of traditional and state-of-the-art data-driven counterparts. To ensure fairness and clarity, all deep learning architectures are calibrated to the same parameter count. Our evaluation assesses not only predictive accuracy but also physical plausibility and robustness to sensor noise.
- Moreover, we validate the practical utility of our methodology through a transfer learning study, assessing the generalizability of the best-performing model on a new, unseen temperature dynamics.

2. Methodology

The methodological approach of this study, depicted in Figure 1, is designed to predict temperature dynamics in the pharmaceutical lyophilization process.

We formulate a piecewise linear function that approximates the ideal temperature evolution of the freeze-drying process to serve as the Process-Informed (PI) prior. The PI prior is designed to balance physical realism with practical applicability. While a first-principles model based on thermodynamic equations would offer the highest fidelity, such models are often complex in real-world manufacturing settings. They require numerous

product-specific parameters, e.g. vial heat transfer coefficients, product resistance to mass flow, eutectic temperatures, that vary between products and are not available in historical process data. Therefore, we formulate an effective prior based on the known operational setpoints of the manufacturing recipe. This recipe-informed approach captures the dominant, low-frequency thermal dynamics defined by the process recipe, which provides the main temperature variation. Moreover, since lyophilization is a slow, multi-day process with gradual, controlled phase transitions, linear approximations of the ramps and holds are a reasonable and effective simplification. Our piecewise linear function models the idealized temperature trajectory as a series of ramps and holds corresponding to the freezing, primary drying and secondary drying phases.

$$y(t) = \begin{cases} y_0 + \frac{y_1 - y_0}{t_1 - t_0}(t - t_0), & \text{for } 0 \leq t < t_1 \quad (\text{freezing}) \\ y_1, & \text{for } t_1 \leq t < t_2 \quad (\text{freezing}) \\ y_1 + \frac{y_2 - y_1}{t_3 - t_2}(t - t_2), & \text{for } t_2 \leq t < t_3 \quad (\text{primary drying}) \\ y_2, & \text{for } t_3 \leq t < t_4 \quad (\text{primary drying}) \\ y_2 + \frac{y_3 - y_2}{t_5 - t_4}(t - t_4), & \text{for } t_4 \leq t < t_5 \quad (\text{secondary drying}) \\ y_3, & \text{for } t_5 \leq t < t_6 \quad (\text{secondary drying}) \end{cases} \quad (1)$$

Here, y_0, y_1, y_2 , and y_3 represents the temperature setpoints at the start of each main process phase, while t_0, t_6 corresponds to the start and end times of the lyophilization cycle. The intermediate time values t_1, t_2, \dots, t_5 define the transition boundaries between the sub-phases, including the ramp-up, hold, and transition periods. These parameters are derived directly from the manufacturing process recipe, representing the intended temperature setpoints and phase transition times. This formulation allows for the generation of a continuous, piecewise-linear target trajectory that captures the dominant thermal structure of the lyophilization process and reflects practical operating constraints. This function is used as a process-informed prior for post-hoc integration for classical models, and in the learning process of deep learning models.

We explore different loss function formulations. In classical models, we define the PIF as a convex combination of the model output $\hat{y}_{\text{classic},i}$ and the process-informed prior $y(t_i)$. This is controlled by two non-negative weights, α and β , which determine the importance of the data-driven and process-

informed components:

$$\hat{y}_{\text{PIF_classic},i}(\alpha, \beta) = \frac{\alpha \cdot \hat{y}_{\text{classic},i} + \beta \cdot y(t_i)}{\alpha + \beta} \quad (2)$$

Here, α is the trust in the classical model's prediction while β reflects the confidence of the process-informed prior. The normalization by $\alpha + \beta$ ensures the result is a weighted average between the two extremes. The optimal coefficients α and β are selected by minimizing the Root Mean Square Error (RMSE) on a validation set:

$$(\alpha^*, \beta^*) = \arg \min_{\alpha, \beta} \sqrt{\frac{1}{M} \sum_{j=1}^M (y_{\text{val},j} - \hat{y}_{\text{PIF_classic},j}(\alpha, \beta))^2} \quad (3)$$

For deep learning models, we investigate three distinct loss function formulations, progressing from a static weighting to more sophisticated dynamic schemes. First, we implement a fixed-weight loss function defined as

$$\mathcal{L}_{\text{fixed}} = (1 - \lambda) \cdot \mathcal{L}_{\text{data}} + \lambda \cdot \mathcal{L}_{\text{PI}} \quad (4)$$

Here, $\mathcal{L}_{\text{data}}$ is the standard supervised loss defined as the Mean Squared Error (MSE) between the model's prediction \hat{y}_i and the ground truth sensor reading $y_{\text{true},i}$. Instead, the process-informed loss \mathcal{L}_{PI} measures the MSE between the model's prediction and the idealized trajectory prior $y_{\text{PI}}(t_i)$. For a batch of size N , these terms are:

$$\mathcal{L}_{\text{data}} = \frac{1}{N} \sum_{i=1}^N (\hat{y}_i - y_{\text{true},i})^2 \quad \mathcal{L}_{\text{PI}} = \frac{1}{N} \sum_{i=1}^N (\hat{y}_i - y_{\text{PI}}(t_i))^2. \quad (5)$$

The hyperparameter λ is determined empirically and sets a static trade-off between data fidelity and process-informed consistency for the entire training process. Here, λ is systematically optimized using the Optuna framework for automated hyperparameter search [33]. This approach ensures that the chosen value for λ is optimal with respect to the validation data, rather than being selected through manual trial and error.

Second, we employ a homoscedastic uncertainty-weight loss, which dynamically balances the data-driven and process-informed terms. Inspired by

Kendall et al. (2018) [31], this approach learns the optimal global balance by interpreting the loss weights as learnable uncertainty parameters:

$$\mathcal{L}_{\text{uncertainty}} = \frac{1}{2\sigma_{\text{data}}^2} \mathcal{L}_{\text{data}} + \frac{1}{2\sigma_{\text{PI}}^2} \mathcal{L}_{\text{PI}} + \log \sigma_{\text{data}} \sigma_{\text{PI}}, \quad (6)$$

where σ_{data} and σ_{PI} represent the learnable homoscedastic uncertainty parameters associated with the data-driven and process-informed components, respectively. The model learns an optimal σ for each loss component across the entire dataset. The final \log term acts as a regularizer that penalizes the model from increasing uncertainty, preventing it from ignoring the tasks entirely. This formulation allows the model to learn an optimal trade-off during training, while avoiding expensive and often sub-optimal manual hyperparameter tuning.

Third, we explore a Residual-Based Attention (RBA) scheme, a gradient-less and computationally efficient method for assigning dynamic, local weights to individual points in the loss calculation [32]. The RBA scheme updates the weights for each point at every training step based on an exponentially weighted moving average of its normalized residual:

$$\lambda_{\text{data},i}^{k+1} \leftarrow (1 - \eta) \lambda_{\text{data},i}^k + \eta \cdot |\hat{y}_i^k - y_{\text{true},i}^k| \quad \lambda_{\text{PI},i}^{k+1} \leftarrow (1 - \eta) \lambda_{\text{PI},i}^k + \eta \cdot |\hat{y}_i^k - y_{\text{PI},i}^k| \quad (7)$$

Here, \hat{y}_i^k is the model’s prediction for sample i at iteration k , while $y_{\text{true},i}^k$ and $y_{\text{PI},i}^k$ are the corresponding ground truth and process-derived target. The hyperparameter η serves as a learning rate that controls the responsiveness of the weights to recent errors. To ensure a stable trade-off, these raw attention weights are normalized for each sample before being used in the final loss computation. The loss function for a batch of size B is formulated as the mean of these dynamically weighted loss terms:

$$\mathcal{L}_{\text{RBA}} = \frac{1}{B} \sum_{i=1}^B [w_{\text{data}}(i) \cdot (\hat{y}_i - y_{\text{true},i})^2 + w_{\text{PI}}(i) \cdot (\hat{y}_i - y_{\text{PI},i})^2], \quad (8)$$

where the normalized weights are given by:

$$w_{\text{data}}(i) = \frac{\lambda_{\text{data}}(i)}{\lambda_{\text{data}}(i) + \lambda_{\text{PI}}(i)}, \quad w_{\text{PI}}(i) = \frac{\lambda_{\text{PI}}(i)}{\lambda_{\text{data}}(i) + \lambda_{\text{PI}}(i)}. \quad (9)$$

This formulation dynamically increases the influence of the loss components with the highest residual for each specific sample, guiding the optimizer to

focus on the most critical points and process domains without incurring significant computational overhead.

We also analyze classical time-series forecasting models, including ARIMA, ETS, Linear Regression, and Kalman Filters. These models are effective for linear, seasonal, or trend-dominated behavior, which is common in many industrial processes. Second, the evaluated deep learning models are standard Recurrent Neural Networks (RNNs), LSTM networks, and attention-based Transformers, as well as recent approaches, such as KANs, cKAN, and LEM. Each of these methods integrates process-informed constraints into the learning process, addressing limitations of pure data-driven approaches.

All deep learning models are trained and tuned to have approximately the same number of parameters to ensure a fair comparison. We evaluate models across predictive accuracy and physical plausibility over a test set of size M . Predictive accuracy is quantified through the Root Mean Square Error (RMSE), which measures the standard deviation of the prediction error:

$$\text{RMSE} = \sqrt{\frac{1}{M} \sum_{j=1}^M (\hat{y}_j - y_{\text{true},j})^2} \quad (10)$$

To capture worst-case performance, which is critical for identifying models that may produce large deviations, we also compute the L-infinity error ($L_\infty(\text{RMSE})$), defined as the maximum absolute prediction error across the test set:

$$L_\infty(\text{RMSE}) = \max_j |\hat{y}_j - y_{\text{true},j}|. \quad (11)$$

Moreover, the physical plausibility of the forecast is assessed via the Gradient Error. This metric quantifies how well the model captures the process dynamics by measuring the average absolute difference between the numerical gradients of the predicted and true time series:

$$\text{GradientError} = \frac{1}{M} \sum_{j=1}^M |\nabla \hat{y}_j - \nabla y_{\text{true},j}|, \quad (12)$$

where ∇ represents the numerical gradient operator, calculated using central differences. Hence, to measure the worst-case error in the predicted rate of change, we use the L-infinity Gradient Error ($L_\infty(\text{GradError})$), which highlights the single point in time where the model's understanding of the

process dynamics is most inaccurate:

$$L_\infty(\text{GradError}) = \max_j |\nabla \hat{y}_j - \nabla y_{\text{true},j}|. \quad (13)$$

To assess robustness, we perform a noise perturbation analysis. In real-world manufacturing processes, sensor readings are rarely perfect due to probe drift, wiring picking up interference, and even ground-truth measurements can have errors. A forecasting model that performs well on clean data may fail when deployed in such a noisy environment, compromising product quality and safety. Therefore, robustness analysis assesses not only how accurately a model fits historical data, but also how reliably it performs when confronted with realistic measurement uncertainty. Thus, Gaussian noise with zero mean and increasing standard deviation, up to $\sigma = 1$, is added to the test set.

We adopt two complementary strategies to assess different facets of robustness. In the first approach, Gaussian noise with increasing standard deviation is added only to the model input, while the target output remains unchanged. This simulates a typical industrial scenario where sensor readings are noisy, but the ground-truth measurements used for evaluation are clean. Models that rely on sequential input, e.g. RNNs, LSTMs, KANs, are directly affected and must learn to predict with the noise. Classical models, which do not condition on input sensor data but instead rely on temporal coordinates, are immune to this perturbation. Thus, their prediction remains unchanged even when noise increases. This behavior is not a fault, but rather a demonstration of their independence from input noise, which can be an advantage in high-noise settings. The main strength of this test is that it isolates the model's internal robustness to input noise. However, it may overstate the reliability of time-conditioned models by not accounting for imperfections in the measured target.

Instead, in the second approach, we add noise to both the inputs and the target values. This models a situation where the sensor reading used for both prediction and evaluation is uncertain. Sequential models will be influenced by both sources. For classical models, while predictions remain constant, the RMSE varies depending on the amount of noise added to the ground truth, since they are being compared to increasingly uncertain targets. This second approach is more realistic for real-world deployments where ground truth values are not perfect. Thus, it is possible to assess not only model stability, but also how reliable the evaluation is in noisy environments. The

disadvantage is that it introduces two sources of error that are intertwined, making it harder to pinpoint the precise cause of performance degradation. Together, these two strategies provide a rich and complementary understanding of model robustness. The first isolates the internal resistance of the model to perturbations. Thus, the second evaluates how well the model performs under noisy operational conditions that affect the entire data pipeline.

Moreover, we extend the analysis to a transfer learning scenario. In pharmaceutical manufacturing, a single equipment is often used for multiple products, each defined by a unique processing recipe. Thus, developing and validating a new forecasting model from scratch for each product is both data-intensive and cost-prohibitive. Transfer learning is a solution allowing a robust pre-trained model to be quickly adapted to a new task with minimal data and computational effort. We tested this capability by selecting the top-performing architecture from the robustness analysis at $\sigma = 0.6$, which is a realistic level of sensor noise [34]. This pre-trained model is then applied to a new, unseen lyophilization dataset to evaluate its ability to adapt and perform in a novel context. We use two different transfer learning strategies to test the model’s adaptability. The first strategy is a baseline, where the pre-trained model is applied to the new dataset without any retraining. This measures the model’s generalization ability. The second strategy tests the reusability of the learned features by freezing the entire pre-trained model and training only a new linear output layer on the new data. This is a computationally efficient way to see if the model’s core has learned a robust representation of the process dynamics.

To further validate the generalizability of our findings, we introduce a secondary lyophilization dataset. This dataset originates from a different pharmaceutical product with a distinct thermal profile, including different temperature setpoints and a longer secondary drying phase. It is partitioned using the same 60/20/20 chronological split for training, validation, and testing. This secondary process serves as a challenging test case to assess whether the conclusions drawn from our primary analysis hold across different manufacturing contexts. The full evaluation metrics for all models on this secondary dataset are provided in Appendix C, Table C.8.

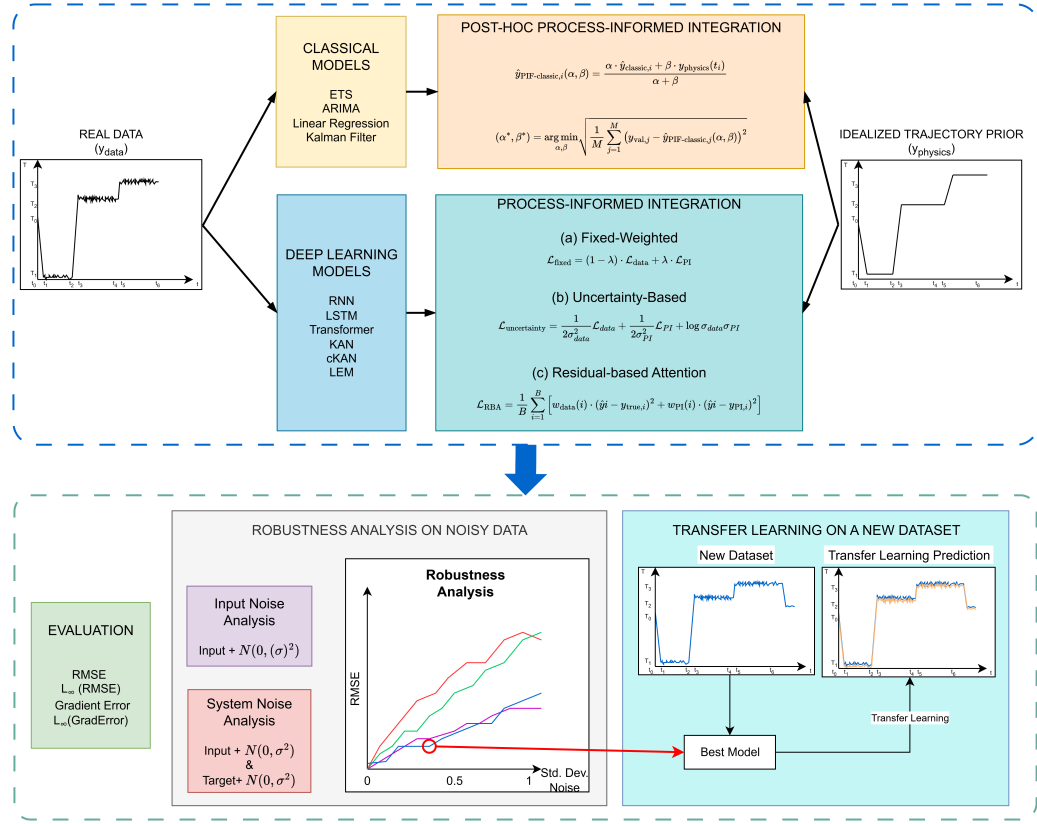


Figure 1: Overview of the proposed Process-Informed Forecasting (PIF) methodology. (Upper part) Real sensor data (y_{data}) are used to train classical and deep learning models. A Process-Informed (PI) prior (y_{PI}), derived from the manufacturing recipe, is then incorporated to create PIF models. Classical Models undergo post-hoc integration. While deep learning models are guided by three distinct loss function formulations: (a) Fixed-Weighted, (b) Uncertainty-Based, and (c) Residual-based Attention (RBA). (Lower Part) The performance of all models, classical, data-driven and PIF models, are assessed through standard metrics of accuracy ($RMSE$, $L_{\infty}(RMSE)$) and physical plausibility ($GradientError$, $L_{\infty}(GradErr)$). Then a robustness analysis under two distinct noise injection scenarios, input-only and system-wide, is performed. Finally, a transfer learning task evaluates the generalizability of the best-performing model by applying it to a new, unseen dataset.

3. Results and Discussion

3.1. Classical Time-Series Models

ARIMA, ETS, Kalman Filter, and Linear Regression are tested in their standard form and in a process-informed version. Through a validation-

based grid search, the optimal configuration for the PI version is $\alpha = 0.7$ and $\beta = 0.3$. This weighting minimizes RMSE on the validation set and is applied consistently across all PI variants. The performance of the classical forecasting models is summarized in Table 1. The results show a trade-off between predictive accuracy and physical plausibility. In terms of pure forecasting accuracy, the standard models achieve a lower $RMSE$ and $L_\infty(RMSE)$. Instead, the PIF models ($_fixed$), which incorporate the process-informed prior, achieve a lower Gradient Error and $L_\infty(GradError)$. Thus, PIF models generate forecasts that are more aligned with the process dynamics.

Table 1: Comparison of metrics for classical time-series models and their PIF variants. The weights $\alpha = 0.7$, $\beta = 0.3$ were selected to minimize RMSE on a validation set. Standard models outperform their process-informed versions in terms of forecasting accuracy, achieving the lowest RMSE and $L_\infty RMSE$ value. Instead, PIF models, which incorporate process prior, achieve better alignment with the process dynamics, achieving lower Gradient Error and $L_\infty GradError$. Training time is comparable across variants for each model family.

Model	RMSE	$L_\infty(RMSE)$	GradientError	$L_\infty(GradErr)$	TrainingTime(s)
ARIMA Models					
ARIMA	0.00472	0.03090	0.00148	0.01801	2207.4
ARIMA $_fixed$	0.00730	0.04930	0.00133	0.01743	2196.3
ETS Models					
ETS	0.00466	0.03712	0.00144	0.01840	840.9
ETS $_fixed$	0.00796	0.04863	0.00133	0.01725	841.4
Linear Regression Models					
LinearRegression	0.00483	0.03618	0.00165	0.02786	0.109
LinearRegression $_fixed$	0.00833	0.05396	0.00145	0.02168	0.195
Kalman Filter Models					
KalmanFilter	0.00537	0.03124	0.00185	0.01729	0.335
KalmanFilter $_fixed$	0.00846	0.04655	0.00161	0.01691	0.339

3.2. Deep Learning Models

Our investigation involves benchmarking seven families of deep learning models and their PIF variants across three levels of complexity: approximately 15,000, 30,000, 45,000 and 115,000 parameters. The detailed results, presented in Table B.6, Table 2, Table B.7 and Table 3, provide insights regarding the interaction between model capability, architecture, and PI integration. First, as the model size increases, the process-informed integration becomes more accurate. At the 15,000 parameter scale, different data-driven models (e.g. cKAN, KAN, MLP) have the lowest RMSE. However, as the parameter count grows to 30,000, 45,000 and 115,000 parameters, PIF models outperform their data-driven counterparts in terms of accuracy. At 115,000 parameters, a PI variant is the top performer in almost every model family. Thus, the process-informed prior is a strong regularizer, preventing the higher capacity models from overfitting to the noise in the training data and

guiding them towards more generalizable solutions. Moreover, while no single PIF strategy is universally superior across all architectures, the fixed-weight strategy (fixed) is often effective (e.g. for LEM and cKAN at 45,000 parameters). However, this strategy requires high computational cost due to the extensive hyperparameter search required by Optuna. For complex models like KAN and LEM, this results in training times that are orders of magnitude longer than their data-driven counterparts. On the other hand, the uncertainty-based (uncertainty) and residual-based attention (RBA) methods are competitive and faster compared to the pure data-driven models. This makes them highly attractive candidates for real-world applications. The uncertainty-based models frequently rank among the best performers (e.g., for RNN and LSTM), offering a scalable approach to PIF methodology. Figure 2 provides a qualitative view of these performance differences for the top-performing models at the $\sim 30,000$ parameter scale. While most models accurately track the stable phases, the zoom-in section reveals distinctions during the rapid temperature ramps. Architectures like cKAN and KAN demonstrate a strong ability to capture these sharp transients, closely following the ground truth. In contrast, the Transformer model fails to reach the peak temperature, visually confirming the limitations suggested by its higher Gradient Error metrics.

Table 2: Performance evaluation of deep learning models and their PIF models, with model complexity increased to approximately 30,000 parameters. By increasing the number of parameters, several process-informed models outperform their standard data-driven counterparts in predictive accuracy (RMSE). Uncertainty-based PIF variant is the top performer for the RNN family, fixed-weighted models lead for LSTM and LEM, and the RBA strategy is the most accurate for the transformer. Uncertainty-based models and RBA methods confirm the computational efficiency trend offering the fastest training times. Instead, the fixed-weighted strategy is accurate but often comes with a huge increase in training time (KAN, LEM).

Model Family	RMSE	$L_\infty(RMSE)$	GradientError	$L_\infty(GradError)$	TrainingTime(s)
RNN Models					
RNN_ uncertainty	0.00643	0.03327	0.00190	0.01634	7.23
RNN_ RBA	0.00846	0.03501	0.00193	0.01544	8.71
RNN_	0.00969	0.03951	0.00189	0.01639	12.16
RNN_ fixed	0.00998	0.03784	0.00187	0.01500	155.81
cKAN Models					
cKAN	0.00859	0.07052	0.00167	0.01454	9.87
cPKAN_ fixed	0.00943	0.05493	0.00165	0.01580	109.90
cPKAN_ RBA	0.01991	0.08864	0.00170	0.01758	9.64
cPKAN_ uncertainty	0.02048	0.12575	0.00179	0.01534	6.42
KAN Models					
KAN	0.00932	0.04662	0.00204	0.01892	1835.93
PKAN_ fixed	0.00939	0.04797	0.00204	0.01890	29389.34
PKAN_ uncertainty	0.01466	0.09402	0.00194	0.02023	1808.68
PKAN_ RBA	0.01479	0.10607	0.00207	0.02093	1963.26
LEM Models					
LEM_ fixed	0.00879	0.07897	0.00177	0.01530	29684.63
LEM_ RBA	0.01034	0.06104	0.00183	0.01583	2537.36
LEM_ uncertainty	0.01154	0.06504	0.00174	0.01621	1448.92
LEM_	0.01190	0.08645	0.00181	0.01565	1447.18
LSTM Models					
LSTM_ fixed	0.00969	0.05686	0.00194	0.01543	185.46
LSTM_	0.01065	0.07347	0.00193	0.01560	15.59
LSTM_ RBA	0.01119	0.05980	0.00201	0.01497	13.65
LSTM_ uncertainty	0.01122	0.06223	0.00198	0.01534	10.01
MLP Models					
MLP	0.00970	0.06602	0.00172	0.01811	10.27
MLP_ uncertainty	0.01513	0.08343	0.00179	0.01888	10.30
MLP_ fixed	0.01694	0.12101	0.00181	0.01920	102.37
MLP_ RBA	0.01772	0.08578	0.00177	0.01847	8.60
Transformer Models					
Transformer_ fixed	0.01651	0.06585	0.00147	0.02582	647.75
Transformer_ RBA	0.01723	0.09773	0.00158	0.03970	66.83
Transformer_ uncertainty	0.01993	0.12053	0.00154	0.01707	31.58
Transformer	0.02057	0.11899	0.00151	0.02849	46.78

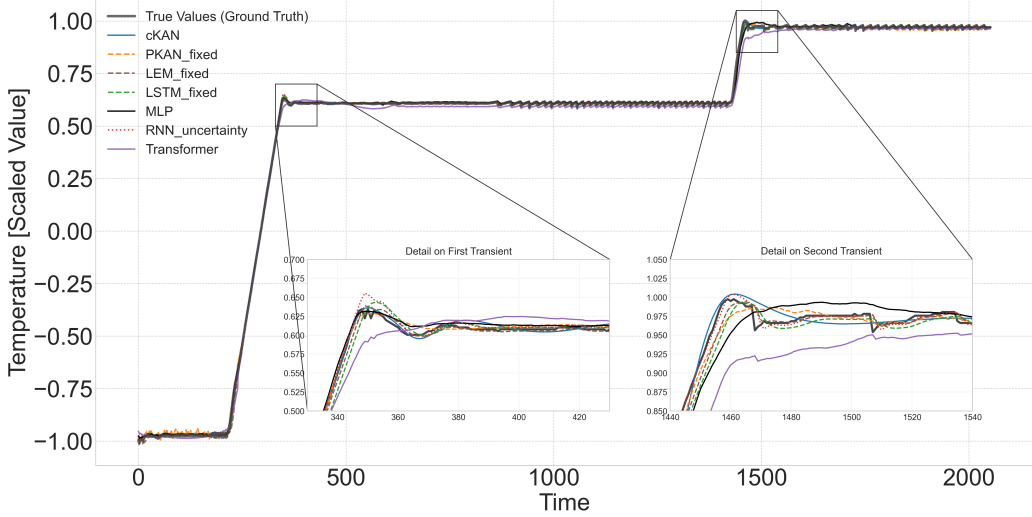


Figure 2: Comparative analysis of model predictions for the thermal dynamics of the lyophilization process. The figure shows the output of the best-performing variant from seven different model families ($\sim 30,000$ parameters). While all models perform well during stable phases, the insets zoom in on the two main temperature ramps to reveal key differences in dynamic response. These zoomed-in views highlight the effectiveness of architectures like cKAN, KAN and LEM in modeling non-linear, transient behavior. In contrast, the Transformer architecture struggles to capture the peak temperature, underscoring its limitations for this specific dynamic system.

Table 3: Performance metrics for high-capacity models (approx. 115,000 parameters). The results show that increasing model capacity does not guarantee better performance. At this scale, the regularizing effect of adaptive PIF strategies becomes more visible, with the RNN_uncertainty and LEM_RBA models leveraging as top performers. The results also underscore the computational cost of the fixed-weight strategy for complex models like KAN.

Model	RMSE	Linf	RMSE	GradientError	Linf	GradError	TrainingTime(s)
RNN Models							
RNN_uncertainty	0.00863	0.05838	0.00186	0.01640			13.08
RNN_fixed	0.00946	0.06115	0.00191	0.01463			22.74
RNN_RBA	0.01112	0.05961	0.00194	0.01494			16.60
RNN_fixed	0.01135	0.04987	0.00197	0.01474			249.07
KAN Models							
KAN	0.00888	0.04923	0.00192	0.01734			6318.68
PKAN_fixed	0.00911	0.05502	0.00193	0.01741			104168.62
PKAN_uncertainty	0.01409	0.09684	0.00175	0.01609			6422.59
PKAN_RBA	0.01469	0.10648	0.00188	0.01679			7820.95
LEM Models							
LEM_RBA	0.00930	0.06211	0.00192	0.01601			3611.39
LEM_fixed	0.00961	0.08928	0.00188	0.01522			2279.18
LEM_fixed	0.00989	0.08874	0.00188	0.01496			42803.50
LEM_uncertainty	0.01264	0.06196	0.00182	0.01643			2228.67
MLP Models							
MLP_Ffixed	0.01200	0.08830	0.00176	0.01891			120.67
MLP_fixed	0.01405	0.08326	0.00188	0.01835			13.51
MLP_uncertainty	0.01439	0.08380	0.00173	0.01829			9.60
MLP_RBA	0.01630	0.08129	0.00173	0.01856			10.94
LSTM Models							
LSTM_fixed	0.01260	0.08385	0.00208	0.01590			286.78
LSTM_RBA	0.01300	0.10527	0.0216	0.01814			25.23
LSTM_uncertainty	0.01374	0.09521	0.0210	0.01659			21.89
LSTM_fixed	0.01410	0.12809	0.0211	0.01540			23.06
Transformer Models							
Transformer_RBA	0.01192	0.08486	0.00145	0.01586			87.30
Transformer_uncertainty	0.01259	0.07800	0.00155	0.01581			78.05
Transformer_fixed	0.01376	0.07045	0.00151	0.03476			1006.42
Transformer	0.02474	0.12985	0.00143	0.04371			35.25
cKAN Models							
cPKAN_RBA	0.02375	0.17894	0.00193	0.02067			3.84
cPKAN_fixed	0.05427	0.10030	0.00193	0.02122			72.61
cPKAN_uncertainty	0.08643	0.29094	0.00249	0.01874			2.51
cPKAN_fixed	0.09798	0.40427	0.00200	0.02027			4.73

3.3. Robustness Analysis

We have conducted a robustness analysis to assess the models' reliability under realistic operational conditions. We have first evaluated model robustness to input-only noisy sensor readings. Figure 3 shows the performance degradation of the best performing model from each family at 30,000 parameters as a function of increasing input noise. The results identify the cKAN model as the most resilient with the lowest RMSE across the noisy spectrum. KAN and MLP also demonstrate strong robustness. While KAN and MLP also demonstrate strong robustness, architectures such as LEM and Transformer with PI priors are more sensitive to input perturbation. Table 4 provides a detailed numerical breakdown at a plausible industrial environment level of noise ($\sigma = 0.6$) [34], confirming that cKAN not only has a low average error (RMSE) but also excels at capturing the system's rate of

change (Gradient Error).

To provide a qualitative illustration of the results, Figure 5 compares the models’ predictions directly on a noisy input signal. The cKAN model effectively filters the high-frequency noise, reconstructing a smooth prediction that closely follows the noise-free ground truth. In contrast, the predictions from the RNN model become highly volatile, indicating that it is overfitting to the noise. To test if these findings are specific to our primary process, we have performed the same input noise analysis on the secondary lyophilization dataset. The results, detailed in Appendix C (Figure C.8, Table C.9) reveal a consistent but slightly different pattern. While the same group of architectures (MLP, KAN-family) remains the most robust, the MLP model demonstrates the best overall resilience on this secondary process. It suggests that while certain architectures are inherently more robust, the optimal choice can be process-dependent. Figure 4 shows a detailed breakdown for each model family. The classical models are immune to input noise, as their predictions are not conditioned on sensor inputs. For the deep learning families, the performance curves of the different variants are often clustered, confirming that the base architecture is the main factor of noise robustness. Moreover, we have conducted a system-wide noise analysis on the primary dataset, where noise is added to both the input and the target values 6. This scenario shows that when the evaluation target is also uncertain, the performance differences between the top architectures become less pronounced, though the MLP, cKAN, and KAN models remain clustered as the most robust group.

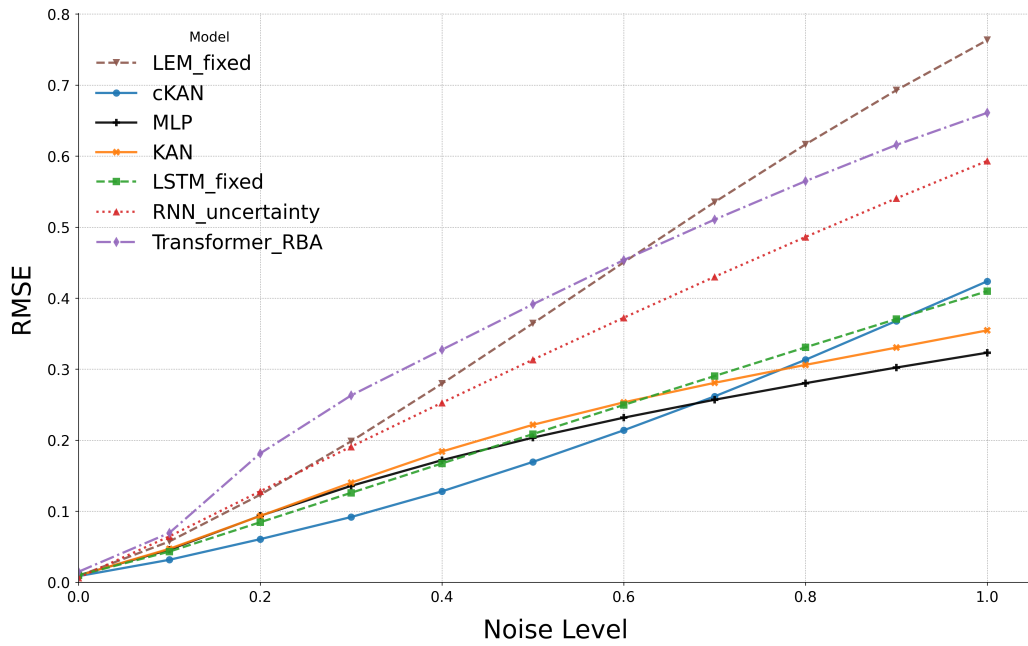


Figure 3: Robustness evaluation of model of approximately 30,000 parameters. This chart evaluates how the predictive accuracy of different models deteriorates as the input data becomes noisier. The results identify the cKAN model as the most resilient maintaining the lowest error across the noise spectrum. The standard KAN and MLP demonstrate strong ability to handle noise. Instead, architecture like LEM_fixed and Transformer_RBA are more sensitive to data perturbations, showing a rapid decline in accuracy as noise level increase.

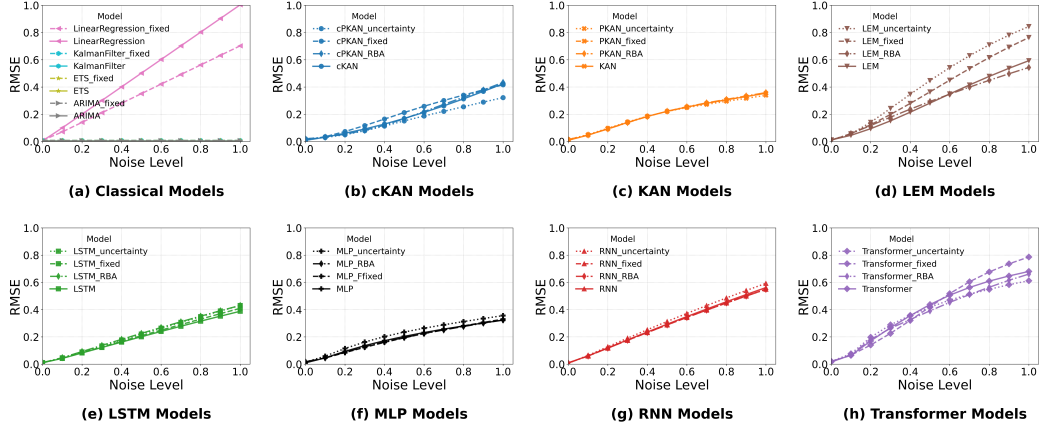


Figure 4: A detailed comparison of model robustness to input noise, with performance degradation (RMSE) analyzed separately for each model family. (a) classical time-series models like ARIMA, ETS and Kalman Filter show immunity to this type of noise. This is an inherent property of these models, as their predictions are based on temporal coordinates, not on the potentially noisy sensor inputs. For deep learning architectures, including (c) KAN, (e) LSTM, (f) MLP, (g) RNN, the performance curves for the standard models and their process-informed variants are clustered, suggesting that the core architecture itself is the primary determinant of resilience to input noise. The Uncertainty-based method is more resilient for models like (b) cKAN and (h) Transformer showing a flatter degradation curve. While for the LEM (d) architecture the standard model proves to be the most resilient.

Table 4: A detailed numerical breakdown of model performance at the 0.60 input noise level. The table evaluates both predictive accuracy (RMSE) and the ability to model system dynamics (Gradient Error). The results highlight the robustness of the cKAN architecture, which achieves the lowest average error and provides the most accurate estimation of the system’s rate of change. This contrast with the MLP, which manages to avoid large individual errors more effectively, as shown by its $L_\infty(RMSE)$ score, suggesting a trade-off between average accuracy and worst-case performance.

Noise Level: 0.60				
Model	RMSE	$L_\infty(RMSE)$	GradientError	$L_\infty(GradError)$
cKAN	0.213913	0.902854	0.073044	0.496527
MLP	0.231686	0.880614	0.111963	0.618187
LSTM_fixed	0.249579	1.043827	0.137960	0.716451
PKAN	0.253263	1.022927	0.121939	0.645686
RNN_uncertainty	0.372449	1.170322	0.210112	0.864049
LEM_fixed	0.450396	1.416625	0.157399	0.784851
Transformer_RBA	0.453573	1.883643	0.153966	1.028948

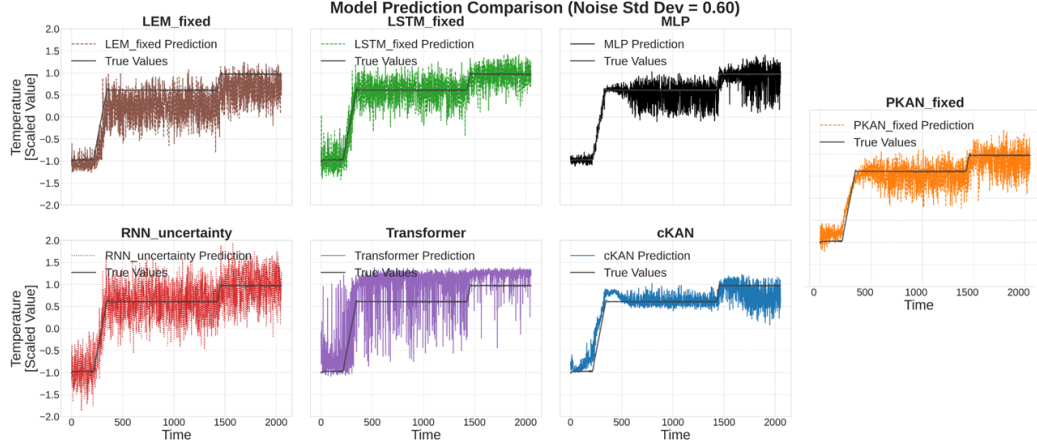


Figure 5: Model prediction comparison on noisy data (Noise $\sigma = 0.6$). This figure shows the prediction of the best-performing models from each family ($\sim 30,000$) parameters on a test set where the input features are corrupted with Gaussian Noise ($\sigma = 0.6$). The predictions are plotted against the original, noise-free ground truth to assess noise-filtering capability. The cKAN model proves to be robust, capable of ignoring fluctuations and predicting the true process state. In contrast, Transformer and RNN predictions indicates high variance making them unsuitable for critical control and monitoring tasks.

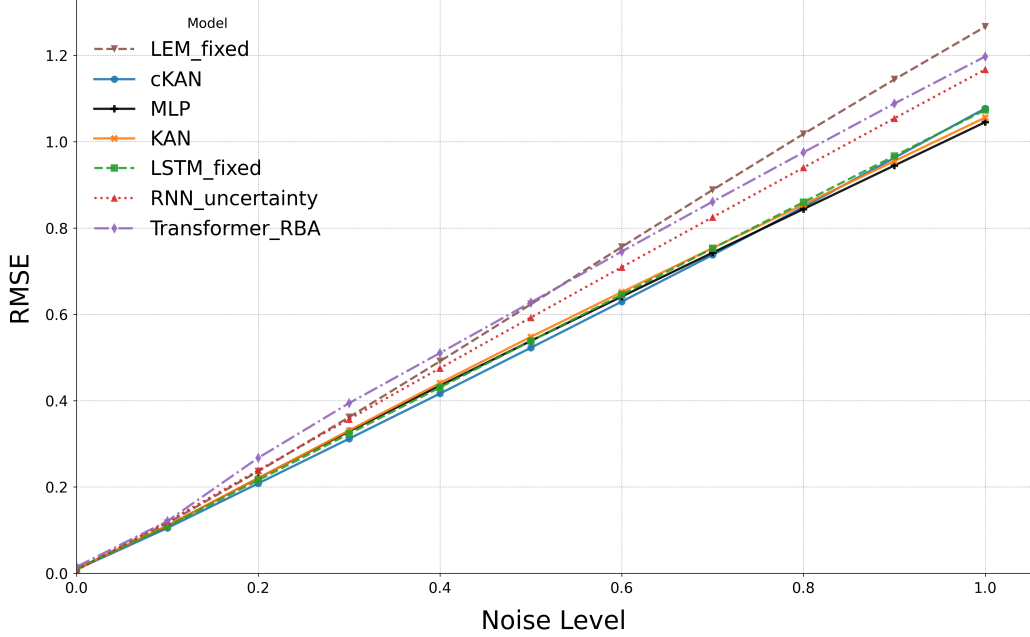


Figure 6: System-wide noise robustness evaluation of model of approximately 30,000 parameters. This chart illustrates how the performance (RMSE) of top models degrades when Gaussian noise is simultaneously added to both the input features (X) and the target values (y). The most robust models - MLP, cKAN, KAN - are clustered. Unlike the input-only noise test where model performance diverged significantly, this scenario shows that when the evaluation target is also noisy, the differences in resilience between top architectures become less pronounced.

3.4. Transfer Learning for Process Adaptability

For the final transfer learning phase, we have selected the best-performing robust model from our primary analysis, the pure cKAN with 30,000 parameters. This choice simulates a realistic workflow where a model developed and validated on one process is then adapted for a new one. We have applied this pre-trained model to a new, unseen lyophilization dataset for a different pharmaceutical product. This new process shares the same underlying structure describable by the idealized trajectory prior (Equation 1) but has a different set of setpoints and an additional drying phase. Thus, this new dataset makes the transfer learning process a realistic generalization challenge. Two different transfer learning strategies are evaluated to test the model’s adaptability, with the results shown in Table 5. The first strategy, a baseline evaluation, applies the pre-trained model directly to the new data without any retrain-

ing. The second, Fine-Tuning, tests the reusability of the learned features by freezing the pre-trained models and training only its final linear output layer. The results show that the baseline evaluation has the highest RMSE value. Thus, this score confirms that while the model may have learned general dynamics, direct application to a new process without adaptation is insufficient. In contrast, the linear probing strategy achieves a compelling improvement, demonstrating that the frozen layers of the pre-trained cKAN model act as a powerful and highly generalizable feature extractor for lyophilization dynamics. With minimal computational effort, the model produces robust models whose learned features can be efficiently repurposed for new manufacturing lines or products.

Table 5: Performance comparison of transfer learning strategies for the pre-trained cKAN model (30,000 parameters) applied to a new, unseen lyophilization dataset. The results demonstrate the accuracy of the linear probing strategy which significantly reduces the RMSE compared to the Baseline evaluation. This indicates that the pre-trained model acts as a powerful feature extractor, whose learned representations can be repurposed for a new process by only retraining a final linear layer.

TL Approach	RMSE	$L_\infty(RMSE)$	GradientError	$L_\infty(GradError)$	TrainingTime(s)
Fine-Tuning	0.1663	0.5817	0.0048	0.0747	34.40
Baseline Evaluation	0.6369	1.0895	0.0033	0.0588	0.5947

4. Summary

In this work, we address the challenge of developing reliable time-series forecasting models for complex thermal dynamics with high frequency features in pharmaceutical manufacturing. We introduce a Process-Informed Forecasting (PIF) methodology to enhance predictive accuracy and physical plausibility of forecasting models. This effect is highlighted in higher capacity deep learning models, where the PI prior acts as a regularizer, preventing overfitting and guiding the models toward more generalizable solutions. Our key findings are threefold. First, process-informed models outperform their purely data-driven counterparts, especially as model complexity increases. Second, our robustness analysis reveals that the intrinsic architecture of a model, such as cKAN, is a primary determinant of its resilience to sensor noise. Third, the transfer learning study confirms the practical utility of our approach, showing that a pre-trained cKAN model can act as a powerful feature extractor, enabling rapid adaptation to a new manufacturing process with minimal computational effort through a transfer learning strategy. This

research provides a roadmap for developing and validating forecasting solutions that are not only accurate but also robust and physically consistent, paving the way for the broader adoption of advanced machine learning in regulated, high-stakes industrial environments.

Credit Authorship Contribution Statement

Ramona Rubini: Writing - original draft, Methodology, Conceptualization, Visualization, Formal analysis, Software, Data curation **Siavash Khodakarami:** Methodology, Formal analysis, Visualization, **Aniruddha Bora:** Methodology, Formal analysis, Visualization, **George Em Karniadakis:** Writing – review and editing, Supervision, Resources, **Michele Dassisti:** Writing – review and editing, Supervision, Project administration, Funding acquisition

Data and Code Availability:

The data and code will be made available after publication at: https://github.com/ramonarubini/process-informed_forecasting.git

Acknowledgements

This work was supported by the Italian Ministry of University and Research under the Programme “Department of Excellence” Legge 232/2016 (Grant No. CUP - D93C23000100001). This work was partially funded also by Sanofi Italia (Grant No. CUP - H91I22000400007). The authors acknowledge the computational resources and services at the Center for Computation and Visualization (CCV), Brown University.

References

- [1] S. L. Nail, S. Jiang, S. Chongprasert, S. A. Knopp, Fundamentals of Freeze-Drying, Springer US, 2002, pp. 281–360. doi:10.1007/978-1-4615-0549-5\6.
- [2] R. Rubini, R. Cassandro, M. Caggiano, C. Semeraro, Z. S. Li, M. Dassisti, The human factor and the resilience of manufacturing processes: a case study of pharmaceutical process toward industry 5.0, in: International Symposium on Industrial Engineering and Automation, Springer, 2023, pp. 96–107.

- [3] R. Rubini, R. Cassandro, C. Semeraro, Z. S. Li, M. Dassisti, Cost-benefit evaluation of digital twin implementation for pharmaceutical lyophilization plant, in: International Conference on Innovative Intelligent Industrial Production and Logistics, Springer, 2023, pp. 398–407.
- [4] G. E. Box, G. M. Jenkins, G. C. Reinsel, G. M. Ljung, Time series analysis: forecasting and control, John Wiley & Sons, 2015.
- [5] E. Storti, L. Cattaneo, A. Polenghi, L. Fumagalli, Customized knowledge discovery in databases methodology for the control of assembly systems, *Machines* 6 (4) (2018) 45.
- [6] E. S. Gardner Jr, Exponential smoothing: The state of the art, *Journal of forecasting* 4 (1) (1985) 1–28.
- [7] C. C. Pegels, Exponential forecasting: Some new variations, *Management Science* (1969) 311–315.
- [8] P. Wang, D. H. Zhang, S. Li, M. W. Wang, B. Chen, Statistical process control based on kalman filter in manufacturing process, *Advanced Materials Research* 201 (2011) 986–989.
- [9] A. L. Korzenowski, M. J. Anzanello, M. S. Portugal, C. Ten Caten, Predictive models with endogenous variables for quality control in customized scenarios affected by multiple setups, *Computers & Industrial Engineering* 65 (4) (2013) 729–736.
- [10] D. Muhr, S. Tripathi, H. Jodlbauer, An adaptive machine learning methodology to determine manufacturing process parameters for each part, *Procedia Computer Science* 180 (2021) 764–771.
- [11] R. Kalman, A new approach to linear filtering and prediction problems, *Journal of Fluids Engineering, Transactions of the ASME* 82 (1) (1960) 35 – 45. doi:10.1115/1.3662552.
- [12] M. Jeffries, E. Lai, J. Hull, Fuzzy flow estimation for ultrasound-based liquid level measurement, *Engineering Applications of Artificial Intelligence* 15 (1) (2002) 31–40.
- [13] A. D. Sowemimo, M. G. Chorzepa, B. Birgisson, Recurrent neural network for quantitative time series predictions of bridge condition ratings, *Infrastructures* 9 (12) (2024) 221.

- [14] C. Cui, J. Chen, Industrial process modeling method using arima-acnn-lstm coupling algorithm, in: *Journal of Physics: Conference Series*, Vol. 2890, IOP Publishing, 2024, p. 012038.
- [15] H. Oukassi, M. Hasni, S. B. Layeb, Long short-term memory networks for forecasting demand in the case of automotive manufacturing industry, in: *2023 IEEE International Conference on Advanced Systems and Emergent Technologies (IC_ASET)*, IEEE, 2023, pp. 01–06.
- [16] A. El Filali, E. H. B. Lahmer, S. El Filali, M. Kasbouya, M. A. Ajouary, S. Akantous, Machine learning applications in supply chain management: A deep learning model using an optimized lstm network for demand forecasting., *International Journal of Intelligent Engineering & Systems* 15 (2) (2022).
- [17] L. Han, M. Abdel-Aty, R. Yu, C. Wang, Lstm + transformer real-time crash risk evaluation using traffic flow and risky driving behavior data, *IEEE Transactions on Intelligent Transportation Systems* 25 (11) (2024) 18383 – 18395. [doi:10.1109/TITS.2024.3438616](https://doi.org/10.1109/TITS.2024.3438616).
- [18] F. Alsaedi, S. Masoud, Condition-based maintenance for degradation-aware control systems in continuous manufacturing, *Machines* 13 (2) (2025) 141.
- [19] H. Abbasimehr, M. Shabani, M. Yousefi, An optimized model using lstm network for demand forecasting, *Computers & industrial engineering* 143 (2020) 106435.
- [20] Y. K. Elalem, S. Maier, R. W. Seifert, A machine learning-based framework for forecasting sales of new products with short life cycles using deep neural networks, *International Journal of Forecasting* 39 (4) (2023) 1874–1894.
- [21] A. Dutta, K. Nath, Learning via long short-term memory (lstm) network for predicting strains in railway bridge members under train induced vibration, in: *ICDSMLA 2020: Proceedings of the 2nd International Conference on Data Science, Machine Learning and Applications*, Springer, 2021, pp. 351–361.

- [22] A. J. Varghese, A. Bora, M. Xu, G. E. Karniadakis, Transformerg2g: Adaptive time-stepping for learning temporal graph embeddings using transformers, *Neural Networks* 172 (2024) 106086.
- [23] A. Zeng, M. Chen, L. Zhang, Q. Xu, Are transformers effective for time series forecasting?, in: *Proceedings of the AAAI conference on artificial intelligence*, Vol. 37, 2023, pp. 11121–11128.
- [24] M. Raissi, P. Perdikaris, G. Karniadakis, Physics-informed neural networks: A deep learning framework for solving forward and inverse problems involving nonlinear partial differential equations, *Journal of Computational Physics* 378 (2019) 686–707. [doi:
https://doi.org/10.1016/j.jcp.2018.10.045](https://doi.org/10.1016/j.jcp.2018.10.045).
- [25] Z. Liu, Y. Wang, S. Vaidya, F. Ruehle, J. Halverson, M. Soljacic, T. Y. Hou, M. Tegmark, KAN: Kolmogorov–arnold networks, in: *The Thirteenth International Conference on Learning Representations*, 2025.
- [26] C. J. Vaca-Rubio, L. Blanco, R. Pereira, M. Caus, Kolmogorov–arnold networks (kans) for time series analysis, *arXiv preprint arXiv:2405.08790* (2024).
- [27] F. Pourkamali-Anaraki, Kolmogorov–arnold networks in low-data regimes: A comparative study with multilayer perceptrons, *arXiv preprint arXiv:2409.10463* (2024).
- [28] S. SS, K. AR, A. KP, et al., Chebyshev polynomial-based kolmogorov–arnold networks: An efficient architecture for nonlinear function approximation, *arXiv preprint arXiv:2405.07200* (2024).
- [29] T. K. Rusch, S. Mishra, N. B. Erichson, M. W. Mahoney, Long expressive memory for sequence modeling, *arXiv preprint arXiv:2110.04744* (2021).
- [30] T. Kapoor, A. Chandra, D. M. Tartakovsky, H. Wang, A. Nunez, R. Dollevoet, Neural oscillators for generalization of physics-informed machine learning, in: *Proceedings of the AAAI Conference on Artificial Intelligence*, Vol. 38, 2024, pp. 13059–13067.
- [31] A. Kendall, Y. Gal, R. Cipolla, Multi-task learning using uncertainty to weigh losses for scene geometry and semantics, in: *Proceedings of*

the IEEE Conference on Computer Vision and Pattern Recognition (CVPR), 2018.

- [32] S. J. Anagnostopoulos, J. D. Toscano, N. Stergiopoulos, G. E. Karniadakis, Residual-based attention in physics-informed neural networks, Computer Methods in Applied Mechanics and Engineering 421 (2024) 116805.
- [33] T. Akiba, S. Sano, T. Yanase, T. Ohta, M. Koyama, Optuna: A next-generation hyperparameter optimization framework, in: Proceedings of the 25th ACM SIGKDD International Conference on Knowledge Discovery and Data Mining, 2019.
- [34] D. Kim, K.-J. Park, Y. Eun, S. H. Son, C. Lu, When thermal control meets sensor noise: analysis of noise-induced temperature error, in: 21st IEEE Real-Time and Embedded Technology and Applications Symposium, IEEE, 2015, pp. 98–107.

Appendix A. Experimental Setup

The framework is implemented in PyTorch and executed on an NVIDIA GPU, leveraging CUDA for computational acceleration. The dataset originates from a real-world pharmaceutical freeze-drying process, with the shelf inlet temperature as the primary target variable. The data is chronologically partitioned into training (60%), validation (20%), and testing (20%) subsets. To prevent information leakage and ensure comparability, all features are normalized to a [-1, 1]. Sequential input vectors for deep learning models are constructed using a lookback window of 300 time steps.

Our evaluation compares a wide spectrum of models, from classical statistical methods (ARIMA, ETS, Kalman Filters, Linear Regression) to deep learning architectures. To ensure a fair and meaningful comparison, all deep learning models are evaluated across three complexity scales with approximately 15,000, 30,000, 45,000 and 115,000 parameters. All deep learning models are trained using the Adam optimizer with an early stopping mechanism based on validation RMSE to prevent overfitting and restore the best-performing weights.

For classical models, a post-hoc integration is performed by finding the optimal convex combination weights (α, β) on the validation set. Deep learning models are evaluated across three complexity scales defined by parameter

counts: approximately 15,000, 30,000, 45,000 and 115,000 parameters. All deep learning models are trained for a maximum of 50 epochs using the Adam optimizer. Learning rates are tailored to the architectures: we use a conservative rate of $5e - 4$ for Transformer models, while all other networks are trained with a rate of $1e - 3$. To prevent overfitting, an early stopping mechanism with a patience of 10 epochs monitored the validation RMSE, terminating training if no improvement is observed and restoring the weights of the best-performing epoch.

Appendix B. Additional Experiments on the First Lyophilization Process

Table B.6: Performance comparison of seven deep learning model families and their PIF models, Fixed-weight (fixed), Uncertainty-based adaptive (uncertainty) and Residual-Based Attention (RBA), all configured to approximately 15,000 parameters for a fair comparison. The optimal models depends on the specific deep learning architecture. Uncertainty-based models and RBA-based models stand out for their computational efficiency providing a balanced performance profile. Standard models often have the lowest RMSE for architectures like MLP and Transformer, however the PI models have a better balance between accuracy, physical consistency and computational cost.

Model Family	RMSE	$L_\infty(RMSE)$	GradientError	$L_\infty(GradErr)$	TrainingTime(s)
RNN Models					
RNN_fixed	0.00668	0.03459	0.00185	0.01630	151.21
RNN	0.00744	0.03725	0.00182	0.01543	10.77
RNN_uncertainty	0.00812	0.03706	0.00188	0.01533	5.78
RNN_RBA	0.01093	0.04133	0.00189	0.01474	7.15
cKAN Models					
cKAN	0.00870	0.06376	0.00169	0.01527	10.09
cPKAN_fixed	0.01293	0.11720	0.00173	0.01488	118.98
cPKAN_uncertainty	0.01482	0.09913	0.00170	0.01570	9.35
cPKAN_RBA	0.01559	0.10043	0.00164	0.01436	15.93
KAN Models					
KAN	0.00916	0.05009	0.00203	0.02025	969.27
PKAN_fixed	0.00927	0.05018	0.00203	0.02030	14971.27
PKAN_uncertainty	0.01450	0.10330	0.00215	0.01907	966.36
PKAN_RBA	0.01553	0.10653	0.00207	0.02174	1179.96
LEM Models					
LEM_fixed	0.00946	0.08554	0.00187	0.01502	31632.11
LEM	0.01155	0.09568	0.00182	0.01561	2160.76
LEM_uncertainty	0.01181	0.07018	0.00177	0.01617	1827.54
LEM_RBA	0.01184	0.06072	0.00184	0.01526	2511.73
LSTM Models					
LSTM_uncertainty	0.01120	0.06546	0.00201	0.01505	12.30
LSTM	0.01156	0.08203	0.00200	0.01557	14.12
LSTM_fixed	0.01175	0.06556	0.00203	0.01572	161.35
LSTM_RBA	0.01350	0.06764	0.00202	0.01532	20.49
MLP Models					
MLP	0.00978	0.05913	0.00180	0.01790	10.17
MLP_fixed	0.01167	0.07070	0.00182	0.01857	119.52
MLP_uncertainty	0.01501	0.08781	0.00179	0.01817	8.72
MLP_RBA	0.01589	0.09288	0.00182	0.01894	8.67
Transformer Models					
Transformer	0.01437	0.07894	0.00147	0.05189	59.59
Transformer_uncertainty	0.02410	0.10513	0.00156	0.03861	34.27
Transformer_RBA	0.02415	0.14527	0.00165	0.04004	67.37
Transformer_fixed	0.05068	0.16858	0.00153	0.05045	702.61

Table B.7: Performance metrics for deep learning models and their PIF models with model complexity increased to approximately 45,000 parameters. At this increased model capacity, process-informed models outperform their standard data-driven counterparts in predictive accuracy across almost all architectures. The Fixed-weight (fixed) and Uncertainty-based (uncertainty) methods are the top performers, with the lowest RMSE for multiple models like LEM, cKAN and LSTM. The uncertainty-based models are the best balance, often the best or near best and one of the most computationally efficient. This suggests that as model capacity grows, the integration of process knowledge becomes increasingly beneficial, with adaptive methods like uncertainty-based offering the most compelling combination of accuracy and practical scalability.

Model Family	RMSE	$L_\infty(RMSE)$	GradientError	$L_\infty(GradErr)$	TrainingTime(s)
RNN Models					
RNN_ uncertainty	0.00748	0.03056	0.00187	0.01640	6.85
RNN_ RBA	0.007884	0.04033	0.00187	0.01560	9.22
RNN_ fixed	0.00902	0.03616	0.00174	0.01740	179.61
RNN_	0.00944	0.04110	0.00188	0.01670	13.38
KAN Models					
KAN_	0.00795	0.04354	0.00201	0.01604	3191.91
PKAN_ fixed	0.00814	0.04606	0.00201	0.01604	41896.50
PKAN_ uncertainty	0.01500	0.09836	0.00192	0.01730	2517.43
PKAN_ RBA	0.01506	0.10062	0.00205	0.01820	2894.93
LEM Models					
LEM_ fixed	0.00848	0.08470	0.00187	0.01622	28017.89
LEM_	0.00909	0.08205	0.00182	0.01517	2175.46
LEM_ RBA	0.01120	0.05128	0.00179	0.01509	2676.21
LEM_ uncertainty	0.01197	0.05839	0.00180	0.01641	1872.03
cKAN Models					
cPKAN_ fixed	0.00937	0.05316	0.00160	0.01449	127.56
cKAN_	0.01342	0.11112	0.00170	0.01743	10.15
cPKAN_ RBA	0.01642	0.10085	0.00171	0.01616	6.76
cPKAN_ uncertainty	0.03758	0.10279	0.00178	0.01838	3.58
LSTM Models					
LSTM_ uncertainty	0.00978	0.04851	0.00198	0.01553	12.29
LSTM_ fixed	0.01011	0.04970	0.00196	0.01556	179.53
LSTM_	0.01065	0.05712	0.00194	0.01567	14.20
LSTM_ RBA	0.01133	0.06430	0.00197	0.01602	10.06
MLP Models					
MLP_ fixed	0.01108	0.07276	0.00173	0.01821	110.44
MLP_	0.01115	0.07090	0.00177	0.01819	8.35
MLP_ uncertainty	0.01539	0.09214	0.00181	0.01873	10.57
MLP_ RBA	0.01696	0.08146	0.00178	0.01815	10.42
Transformer Models					
Transformer_ uncertainty	0.01422	0.09464	0.00156	0.01788	60.08
Transformer_ fixed	0.01534	0.06021	0.00142	0.02996	762.64
Transformer_	0.01585	0.08777	0.00146	0.03325	50.49
Transformer_ RBA	0.02003	0.11264	0.00161	0.03050	63.60

Appendix C. Validation on a Secondary Lyophilization Process

To assess the generalizability of our findings, we conducted a validation study on a secondary unseen lyophilization dataset. This experiment demonstrates the robustness of our conclusions and evaluates the potential of the top-performing models to adapt to new process dynamics. The analysis focuses on the deep learning models at the 30,000 parameter scale, as they are the most capable architectures from our primary study. The secondary dataset is sourced from a lyophilization cycle for a different biopharmaceutical product with different thermal dynamics, different ramp rates and

phase durations. The data are preprocessed and partitioned using the same methodology as the first dataset to ensure a consistent evaluation framework. All models are retrained from scratch on the new training set and evaluated on the test set.

The results are summarized in Table C.8. The KAN and cKAN families are still state of the art, with the lowest RMSE and show strong function approximation capabilities on new data. The fixed-weight models are competitive, closely following their pure counterparts in accuracy and physical consistency. On this secondary dataset, the Transformer architecture and its fixed-weight variant have the lowest value of Gradient Error. Thus, they are better at capturing the underlying temporal structure and trends of this process, even if their overall point-wise accuracy is lower. A significant finding from this validation study is the performance of the uncertainty-weighted models. These variants are competitive on the source dataset and consistently rank lower on this new process. This means that while the uncertainty-based weighting scheme is effective at optimizing the data-physics trade-off for a specific process, it may be less robust to domain shifts compared to the simpler fixed-weight process-informed integration. The key findings from this validation study are that while the MLP architecture is more robust on this specific process, the overall class of robust models (MLP, KAN-family) remains consistent and the fixed-weight integration shows more stable performance across domains than the uncertainty-based method.

Table C.8: Performance evaluation of deep learning models and their PIF variants, with model complexity increased to approximately 30,000 parameters. The table compares Fixed-weight (_fixed), Uncertainty-based (_uncertainty), and Residual-Based Attention (_RBA) integration strategies against their pure data-driven counterparts. At this increased model capacity, process-informed forecasting models often outperform standard models in predictive accuracy (RMSE).

Model	RMSE	$L_\infty(RMSE)$	GradientError	$L_\infty(GradientError)$	TrainingTime(s)
PKAN Models					
PKAN_fixed	0.00843	0.10189	0.00233	0.03655	19931.43
KAN	0.00869	0.10867	0.00232	0.03762	1998.40
PKAN_uncertainty	0.03585	0.29949	0.00258	0.06929	885.78
PKAN_RBA	0.03722	0.29862	0.00254	0.06175	1400.02
cKAN Models					
cKAN	0.00993	0.12820	0.00220	0.05128	11.94
cPKAN_fixed	0.01184	0.13163	0.00225	0.04819	98.22
cPKAN_RBA	0.03395	0.22665	0.00239	0.05739	8.64
cPKAN_uncertainty	0.03842	0.27647	0.00252	0.06251	6.45
MLP Models					
MLP	0.01013	0.12738	0.00229	0.05657	10.63
MLP_Ffixed	0.01070	0.13054	0.00234	0.05344	113.50
MLP_RBA	0.03550	0.32604	0.00246	0.05967	6.50
MLP_uncertainty	0.03826	0.29419	0.00248	0.06606	5.13
RNN Models					
RNN_fixed	0.01040	0.12207	0.00271	0.04811	139.02
RNN_RBA	0.01188	0.09027	0.00298	0.04908	6.13
RNN	0.01243	0.11077	0.00276	0.04649	16.38
RNN_uncertainty	0.01299	0.10861	0.00293	0.04720	5.04
LSTM Models					
LSTM_fixed	0.01341	0.15443	0.00278	0.05673	166.14
LSTM	0.01417	0.17876	0.00269	0.05646	21.98
LSTM_RBA	0.01793	0.15052	0.00268	0.05884	8.22
LSTM_uncertainty	0.02161	0.21440	0.00252	0.04830	6.10
LEM Models					
LEM	0.01731	0.21918	0.00271	0.05422	7369.74
LEM_uncertainty	0.01968	0.19741	0.00283	0.06044	2549.88
LEM_RBA	0.02123	0.22928	0.00277	0.05606	3543.45
LEM_fixed	0.02658	0.23654	0.00280	0.05652	52622.86
Transformer Models					
Transformer_fixed	0.01957	0.11339	0.00188	0.03940	586.49
Transformer	0.02351	0.13749	0.00197	0.05532	46.70
Transformer_RBA	0.03087	0.23494	0.00206	0.04974	29.21
Transformer_uncertainty	0.03822	0.21621	0.00198	0.03934	21.29

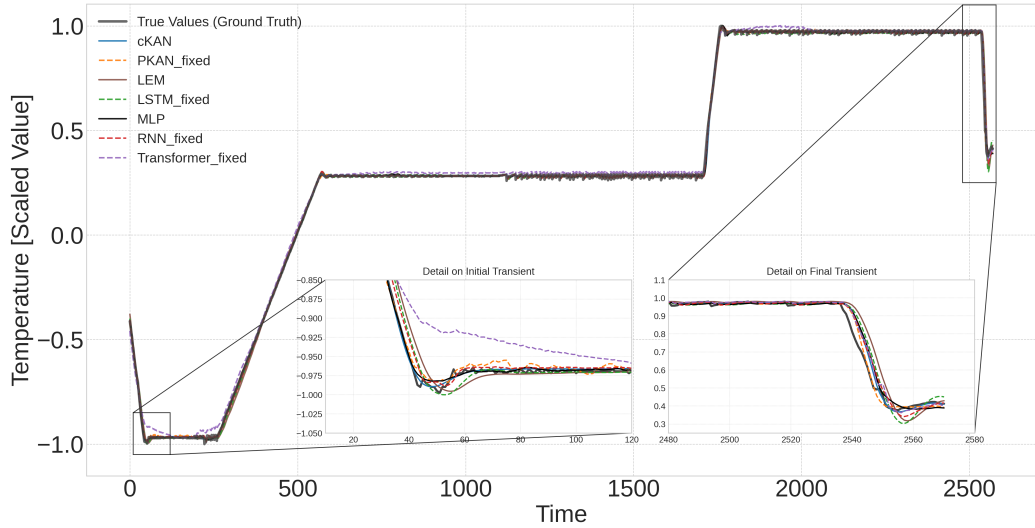


Figure C.7: Comparative analysis of model predictions for the thermal dynamics of the lyophilization process. The figure shows the output of the best-performing variant from seven different model families ($\sim 30,000$ parameters). While all models perform well during stable phases, the insets zoom in on the initial and final transient reveal key differences in dynamic response. These zoomed-in views highlight the effectiveness of architectures like MLP, cKAN, KAN and LEM in modeling non-linear, transient behavior. In contrast, the Transformer architecture struggles to capture the peak temperature, underscoring its limitations for this specific dynamic system.

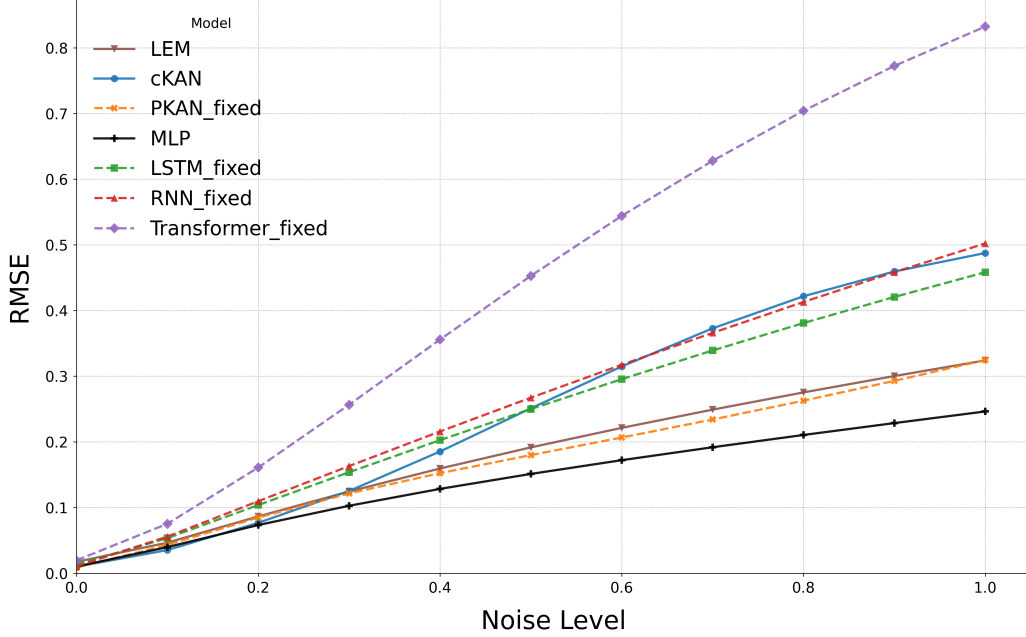


Figure C.8: Robustness evaluation of models of approximately 30,000 parameters on a secondary lyophilization process. This chart evaluates how the predictive accuracy of different models deteriorates as the input data becomes noisier. The results identify the MLP architecture as the most resilient to such perturbations, maintaining the lowest error across all noise levels. The PKAN_fixed model and LEM model also demonstrate strong robustness.

Table C.9: Detailed performance metrics at the 0.60 input noise level. This table provides a quantitative breakdown of performance, evaluating prediction accuracy and system dynamics. The results highlight a performance trade-off: the MLP model is the most robust in terms of overall prediction accuracy, while the cKAN model better captures the instantaneous rate of change.

Noise Level: 0.60				
Model	RMSE	$L_\infty(RMSE)$	GradientError	$L_\infty(GradientError)$
MLP	0.172110	0.684534	0.090911	0.487938
PKAN_fixed	0.206609	0.773152	0.093977	0.503102
LEM	0.221298	1.031625	0.120150	0.628230
LSTM_fixed	0.295458	1.192368	0.160887	0.832902
cKAN	0.314761	0.911930	0.062066	0.410341
RNN_fixed	0.317357	1.238445	0.177930	0.962114
Transformer_fixed	0.544060	1.928450	0.281937	1.018396

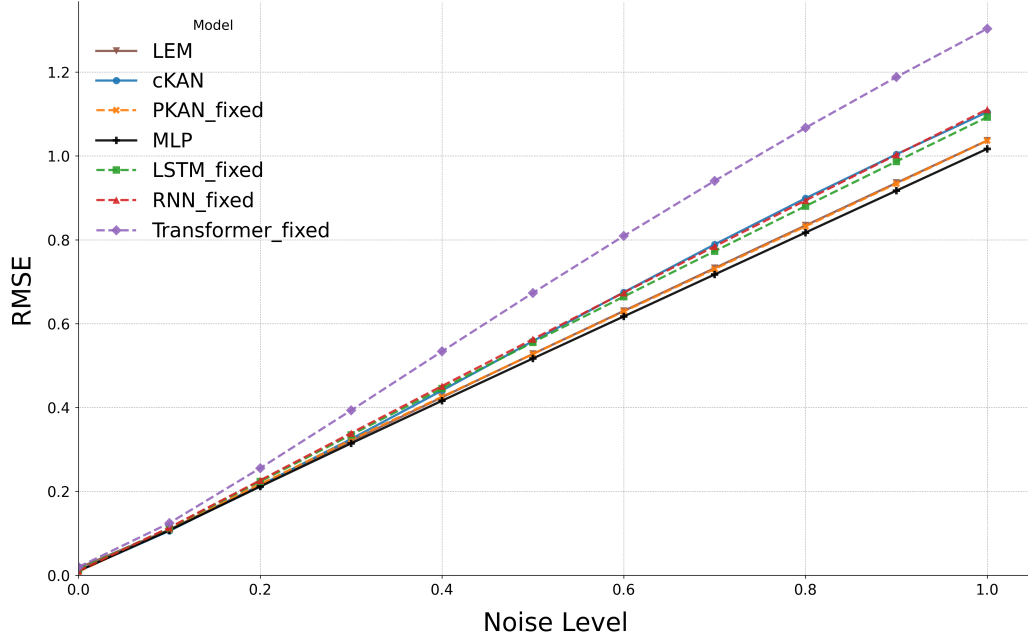


Figure C.9: Robustness evaluation of model of approximately 30,000 parameters on a secondary lyophilization process. This chart evaluates the results of the system noise robustness test, where both input features (X) and the target variable (y) are corrupted with independent, zero-mean Gaussian noise. While the relative performance ranking is consistent with the input noise analysis, with the MLP being the most robust model, the overall performance of all models degrades substantially and more uniformly.

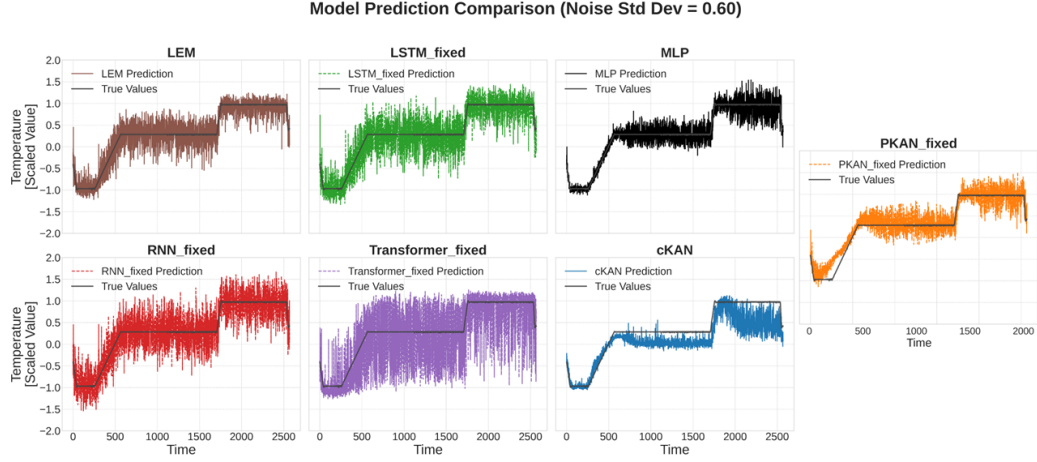


Figure C.10: Model prediction comparison on noisy data (Noise $\sigma = 0.6$). This figure shows the prediction of the best-performing models from each family ($\sim 30,000$) parameters on a test set where the input features are corrupted with Gaussian Noise ($\sigma = 0.6$). The predictions are plotted against the original, noise-free ground truth to assess noise-filtering capability. The MLP model proves to be robust, capable of ignoring fluctuations and predicting the true process state. In contrast, Transformer and RNN predictions indicate high variance making them unsuitable for critical control and monitoring tasks.